Advances in Research
4(3): 179-190, 2015, Article no.AIR.2015.073
ISSN: 2348-0394

SCIENCEDOMAIN *international*
www.sciencedomain.org

Expanding Microwave Confocal Microscope Method through Metamaterials and Modality of Object's Physical Properties

Ahmed M. D. E. Hassanein[1*] and Alonso Corona Chávez[2]

[1]Department of Systems and Information, Engineering Division, National Research Centre (NRC), Dokki, Giza, Egypt.
[2]Department of Electronics, National Institute of Astrophysics, Optics and Electronics (INAOE), Tonantzintla, Puebla, Mexico.

Authors' contributions

This work was carried out in collaboration between both authors. Author AMDEH designed the study, wrote the protocol, and wrote the draft of the manuscript. He managed the literature searches, analyses of the study, writing of the computational simulation programs, plotting the graphs, performing the analysis of the results and drawing the conclusions. Both authors read and approved the final manuscript.

Article Information

DOI: 10.9734/AIR/2015/14996
Editor(s):
(1) Martin Kröger, Computational Polymer Physics, Swiss Federal Institute of Technology (ETH Zürich), Switzerland.
(2) Jinyong Peng, College of Pharmacy, Dalian Medical University, Dalian, China.
Reviewers:
(1) Anonymous, China.
(2) Pierre R. Blanquet, Club d'Histoire des Neurosciences, University P. & M. Curie, Paris, France.
(3) Anonymous, USA.
(4) Bin Wang, Facility Design and Instrumentation Institute, China Aerodynamics Research and Development Center, China.
Complete Peer review History: http://www.sciencedomain.org/review-history.php?iid=969&id=31&aid=8207

Original Research Article

Received 31st October 2014
Accepted 4th February 2015
Published 21st February 2015

ABSTRACT

The quality of tomographic images formed from diffracting waves deteriorated due to the limitations in capturing evanescent waves. The waves carried detailed information about the body being imaged. Metamaterials were being recently used to amplify and focus evanescent waves. Here, the physical characteristics of a superlens made out of a metamaterial slab were studied. A detailed derivation of the equations for wave propagation inside the metamaterial was shown. The effect of changing the real and imaginary parts of the permittivity and permeability of a superlens were examined. The dependence of the cut-off frequency of a superlens on the thickness of the slab was discussed. Suitable physical dimensions of a superlens were proposed for cross sectional imaging

**Corresponding author: E-mail: ahmed22@aucegypt.edu;*

of Aluminum rods. Simulations were done to test the validity of the proposed solution. Simulations showed that a metamaterial slab of Silver could be successfully used in imaging two rods.

Keywords: Tomography; evanescent waves; metamaterials; superlens; perfect Imaging.

NOMENCLATURES

k_x^{cutoff}	*Cutoff frequency.*
k_o	*Value of wave vector in free space.*
d, d_1, d_2, d_3	*Horizontal distance of propagation in slab, medium1, 2 and 3 respectively.*
k_{z1}, k_{z2}, k_{z3}	*Component of the wave vector k in the z direction in medium1, 2 and 3 respectively.*
k_{x1}, k_{x2}, k_{x3}	*Component of the wave vector k in the x direction in medium1, 2 and 3 respectively.*
T, T_1, T_2, T_3	*Total transfer function and transfer function in media1,2 and 3 respectively.*
A, C, E	*Transmission Constant in media1, 2 and 3 respectively.*
B, D	*Reflection Constant in media1 and 2 respectively.*
f_x	*Spatial frequency in the x direction.*
T	*Transmission coefficient.*

GREEK SYMBOLS

$\varepsilon_0, \varepsilon_1, \varepsilon_2, \varepsilon_3$	*Permittivity of free space, medium1, 2 and 3 respectively.*
$\mu_0, \mu_1, \mu_2, \mu_3$	*Permeability of free space, medium1, 2 and 3 respectively.*
ω	*Angular frequency.*
$\varepsilon_r, \varepsilon''$	*Real part and imaginary part of the permittivity respectively.*
ε	*Permittivity equation* $\varepsilon = \varepsilon_r - j\varepsilon''$.
μ_r, μ''	*Real part and imaginary part of the permeability respectively.*
μ	*Permeability equation* $\mu = \mu_r - j\mu''$
λ	*Wavelength used in calculations.*
δ_e	*Ratio of wavevectors multiplied by permittivity.*
Δ	*Resolution of the imaging system.*
δ	*Change in real part of the permittivity.*

ABBREVIATIONS

SPP	*Surface Plasmon Polaritons*

1. INTRODUCTION

Microwave imaging was being widely investigated for medical and process tomography. Problems with resolution when imaging using Ultra Wide Band waves were discussed in several papers [1-3]. For example, the virtual confocal microscope method had been proven theoretically and cross sectional imaging had been demonstrated in [4]. The foundations of this method were the topic of several research investigations including but not limited to a PhD thesis [4]. The method began with a measurement of the wave fronts leaving the target and used these in conjunction with a synthetic optical system to form a confocal image by computing the wave propagation through the effective optics to form the image [4]. Although the results discussed in [4] were satisfactory but the resolution obtained was always dependent upon the size of object being imaged, medium in which the object was located and the wavelength

used. If a wave was incident upon a boundary between two media with an angle greater than the critical angle, evanescent waves were generated or total internal reflection happened. Critical angle was defined using Snell's Law of refraction [5,6]. If a wave was incident on any object, evanescent waves were created as well. The frequency of the scattered evanescent waves was dependent on the shape of the object and the details in it. The more the details were the higher the frequency components which were scattered from the object. Evanescent waves decayed exponentially and couldn't be captured by antennas. The amplitude of a received signal was attenuated and so the quality of calculated images decreased. In addition, due to the diffraction limit [6], an object with dimensions less than half the wavelength used couldn't be imaged. Detailed information about the object being imaged was held by the evanescent waves which couldn't be captured. A metamaterial slab could be used to make the capturing of those waves possible and so the ability to produce a near perfect image for an object possible.

It was shown in [7] that a slab of materials with negative refractive index behaved like a perfect lens focusing all light to an exact electromagnetic copy of an object. For two-dimensional systems, over distances much shorter than the free space wavelength, conformal transformations were applied to the original parallel-sided slab generating a variety of new lenses. Although the new lenses were not 'perfect', they were able to magnify two-dimensional objects. The results applied equally to imaging of electric or magnetic sub-wavelength objects in two dimensions. The concepts had potential applications ranging from microwave frequencies to the visible [7]. The ideas of the perfect lens recently proposed by J.B. Pendry were extended to alternative structures [8-10]. A slab of a medium with negative refractive index bounded by media of different positive refractive index was shown to amplify evanescent waves and could act as a near-perfect lens [10]. In paper [11], transformation-based optics was applied to the derivation of a general class of transparent metamaterial slabs. By means of analytical and numerical full-wave studies, the image displacement/ formation capabilities of transparent metamaterial slabs were explored [11]. The role of such structures in the amplification of the evanescent waves was explained [10]. The image resolution obtained by these lenses was robust against the effects of absorption in the lens. In particular, the case of a slab of silver, was studied, which had a negative dielectric constant, with air on one side and other media such as glass or GaAs on the other side as an example of a near perfect lens [10]. The studies in [10,11] concluded that sub wavelength image resolution was possible. The negative index of refraction in a metamaterial composed of metallic split-ring resonators, which exhibited simultaneously negative permittivity and permeability, was numerically investigated in [12]. A study of open-ring resonators and split-ring resonators was performed in terms of equivalent circuits [13]. The resonant frequencies of five different ring resonators were measured with the aid of a network analyzer within the frequency range of about 1.5 to 2.8 GHz [14]. The experimental and numerical results were shown to be very close to each other [14]. Analytical results from various authors were also compared with the experimental results; one of them led to a large discrepancy, but the other analytical approximations was shown to be not too far off [14]. Also, new periodic structures built with very thin wires had proven to have novel properties not observed before in the GHz band, including some possible impact on superconducting properties [15]. In an effort to practically apply metamaterials, planar hybrid metamaterial with different split ring resonators (SRR) structure dimensions were fabricated on silicon substrates by femtosecond (fs) laser micro-lens array (MLA) lithography and lift-off process [16]. The electromagnetic field responses of these metamaterial structures were characterized using a terahertz (THz) time-domain spectroscopy [16]. The main focus in this paper was to study the conditions required for a metamaterial slab to overcome the problems imposed by evanescent waves and the diffraction limit on perfect imaging.

The aim of this paper was to enhance the resolution limit of an optical system. We used equations which were already known in the literature to design a super lens tailored for the virtual confocal microscope method which was discussed in [4]. This study proposed constructing a super lens through a continuous media that would allow the user to fully control the scattered field from the imaged object. The lens could enable us to significantly enhance the resolution imposed by the diffraction limit [5,17]. Starting with the design process, suitable frequency and size of a super lens were established. A one dimensional super lens was tested to evaluate its performance and compare

the images which were produced by it with the objects being imaged.

2. DESIGN PARAMETERS

In this section, we discussed the effect of changing the real or imaginary parts of the permittivity and permeability of the metamaterial slab. The transfer functions for the free space as well as a slab that was made out of a metamaterial were given. Simulation was done on Matlab™ to examine the performance of a metamaterial slab (transfer functions) when changing permittivity and permeability. Then, we studied the effect of changing the thickness of super lens on the achieved resolution. The change in the cutoff frequency was one of our parameters to quantify the performance of the metamaterial slab when changing any variable. The cutoff frequency was defined as the point at which the value of a transfer function dropped to 0.7 of its initial value.

2.1 Equations Describing Electric Field in Different Media

The slab was represented in Fig. 1 by medium2. The slab was inserted in free space which was represented by medium 1 and 3. The transfer function for free space $T_1(k_{x1})$ was [18]:

$$T_1(k_{x1}) = e^{-j\sqrt{\omega^2\varepsilon_0\mu_0 - k_{x1}^2}\,d_1} \quad (1)$$

Same equation as Eq.1 applied for medium3 where d_1 was replaced by d_3 and k_{x1} was replaced by k_{x3}.

The transfer function for medium2 $T_2(k_{x2})$ was [18]:

$$T_2(k_{x2}) = \frac{4\delta_e}{(1+\delta_e)^2 e^{jkz2d2} - (1-\delta_e)^2 e^{-jkz2d2}} \quad (2)$$

where δ_e was equal to:

$$\delta_e = \frac{k_{z2}\varepsilon_0}{k_{z1}\varepsilon_2}.$$

The total transfer function for the whole three media was:

$$T = T_1(k_{x1}) * T_2(k_{x2}) * T_3(k_{x3}) \quad (3)$$

In the next subsection, Eq. 3 was investigated to study the behavior of the transfer function of the three media collectively as they were defined in Fig. 1. Permeability and Permittivity were the two factors which were going to be the variables in the next subsection.

2.2 Effect of Permittivity and Permeability on Cutoff Frequency

Using Eq. 1, 2 and 3, the attenuation in the amplitude of the transfer function of a metamaterial slab due to losses was shown in the next Figures.

In reference [18], the ideal metamaterial slab that could be used for perfect imaging should have $\varepsilon = -1$ and $\mu = -1$. But in real cases, variation could happen in the values of the permittivity and permeability parameters. We considered the permittivity to be $\varepsilon = \varepsilon_r - j\varepsilon''$ and the permeability to be $\mu = \mu_r - j\mu''$. In the next examples, the effect of the variation in the imaginary part of the permittivity and permeability of the slab on the cut-off frequencies was examined. For this sake, we introduced the parameter d/λ which referred to the thickness of the slab d in terms of the wavelength used λ. In the examples of this subsection, the value $d/\lambda = 0.1$ was assumed. The frequency used was 3GHz.

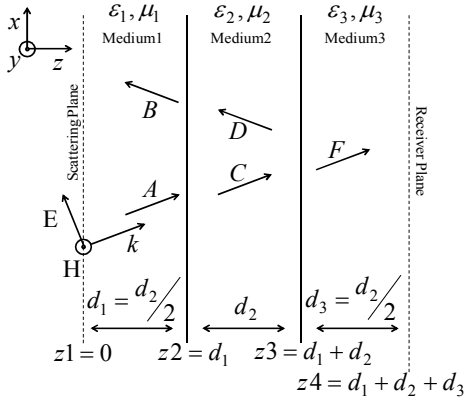

Fig. 1. A sketch not to scale was shown of a superlens (medium 2) inserted in free space (medium 1, 3). The permittivity and permeability of the different media were shown with thicknesses d_1, d_2 and d_3. A TM wave was scattered at the scattering plane and captured at the receiver plane

In Fig. 2a, in the first case it was defined that $\varepsilon = -1 - j\varepsilon''$ where $\varepsilon'' = 10^{-1}$, 10^{-2} or 10^{-3} and $\mu = -1$. The cut-off frequency was calculated using the equation [18]:

$$k_x^{cutoff} \Big/ k_o = (\lambda/(2\pi d))\ln(2/\varepsilon''). \quad (4)$$

The equation of the cut-off frequency was defined when the amplitude of the transfer function (Eq. 3) was equal to 0.7. For a small amount of loss $\varepsilon'' = 10^{-3}$, the transfer function showed a cut-off at $k_x = 12.099k_o$. This meant that a slab of 0.1λ thickness with $\varepsilon = -1 - j0.001$ and $\mu = -1$ reproduced accurately objects with a resolution of $\lambda/12.099$. For $\varepsilon'' = 10^{-2}$, the cut-off frequency reduced to $k_x = 8.434k_o$ and for $\varepsilon'' = 10^{-1}$ to $k_x = 4.768k_o$. The resolution of the slab with $\varepsilon'' = 10^{-2}$ was therefore $\lambda/8.434$ and for $\varepsilon'' = 10^{-1}$ only $\lambda/4.768$. Increasing the loss reduced the resolution. When comparing the three lossy examples with the free space one, the transfer function was seen to be flatter and so more evanescent components could make it to the image plane even for high losses such as $\varepsilon'' = 10^{-1}$. For the propagating components which satisfied $k_x < k_o$, after propagating through the lossy slab their amplitude decreased and so they suffered while the evanescent parts of the waves were amplified when compared to the empty space case. When the slab existed, waves propagated inside the slab for a distance equal to d and then another equivalent distance in free space. But when the slab was absent, waves propagated in free space for a distance equal to $2d$.

In Fig. 2b, the second case was shown in which $\varepsilon = -1$ and $\mu = -1 - j\mu''$ where $\mu'' = 10^{-1}$, 10^{-2} or 10^{-3}. The equation used in this case was [18]:

$$k_x^{cutoff} \Big/ k_o = (\lambda/(2\pi d))\ln\left((4/\mu'') \times \left(k_x^{cutoff} \Big/ k_o\right)^2\right) \quad (5)$$

The cut-off frequencies k_x were $22.738k_o$ for $\mu'' = 10^{-3}$, $19.073k_o$ for $\mu'' = 10^{-2}$ and $15.408k_o$ for $\mu'' = 10^{-1}$. The tendency was the same that was to say increasing the loss reduced the resolution. But, the cut-off frequency was less sensitive to a change in μ'' than was the case for a change in ε''. In the next two cases, the effect of changing the real part of the permittivity on the amplitude of the transfer function (Eq. 3) was explained.

In Fig. 2c, the third case could be seen in which $\varepsilon = -1 - \delta$ where $\delta = 10^{-1}$, 10^{-2} or 10^{-3} and $\mu = -1$. The equation which was used to calculate the cut-off frequency was:

$$k_x^{cutoff} \Big/ k_o = (\lambda/(2\pi d))\ln\left(2 \times \sqrt{3} \Big/ |\delta|\right) \quad (6)$$

In Fig. 2d, the Fourth case was shown in which $\varepsilon = -1 + \delta$ where $\delta = 10^{-1}$, 10^{-2} or 10^{-3} and $\mu = -1$. Same equation as the one which was used in the third case was used for this case as well. For both cases, the cut-off frequencies k_x were $12.974k_o$ for $|\pm\delta| = 10^{-3}$, $9.308k_o$ for $|\pm\delta| = 10^{-2}$ and $5.643k_o$ for $|\pm\delta| = 10^{-1}$. The cut-off frequency exhibited similar characteristics as the examples which were shown before but the transfer function showed resonances in these last two Figures. One resonance was seen in Fig. 2c and two in Fig. 2d.

The scattered waves which were incident on the surface of the slab excited the SPP at the rear side of the slab. The excitation of the SPP modes was undesirable for imaging especially in the case of the less negative ε. The k_x components corresponding to these excitations were represented with amplitudes much higher than those corresponding to non excited modes. In the mean time, these excitations were essential for amplifying the magnitude of the evanescent waves so that they could be detected at the receiver side of the slab [18]. Similar results were seen when a change in the real part of the permeability of the slab was studied.

For the k_x values for which ε_r and μ_r had negative values and their product was smaller

than one, two resonances were seen in the graph. But for the k_x values for which ε_r and μ_r had negative values and their product was larger than one, one resonance was seen in the graph. For this part of the latter frequencies the resonant components in free space were turned into propagating components inside the slab without fulfilling the condition for a resonance that was why only a single resonance was seen [18]. There was a direct correlation between the value of the k_x corresponding to the resonance frequency and the possible achievable resolution [18]. The flat section of the transfer function extended up till the largest value of the k_x corresponding to the excitation of the SPP mode. It could be said that it was the position of this k_x which determined the cut-off frequency of the transfer function [18]. Saying this, the function describing the cut-off frequency was modified to be [18]:

$$k_x^{cutoff} \big/ k_O = \left(\lambda/(2\pi d)\right)\ln\left(2/|\delta|\right). \quad (7)$$

To design a slab, the cutoff frequency was an important quality. The higher the cutoff frequency the more evanescent components could make it to the image plane and so higher resolution could be achieved. The lower the losses in permittivity and permeability were the higher the cutoff frequency. Also, if the real part of permittivity was varied away from one, care should be exercised to use frequencies which didn't cause resonance.

2.3 Resolution of a Metamaterial Slab

If it could be estimated that the resolution Δ was being inversely proportional to the cut-off frequency as could be described in the equation: $\Delta = 2\pi \big/ k_x^{cutoff}$.

Then, after some mathematical manipulation to Eq.(2), it could be deduced that [18]:

$$d = \frac{\Delta}{2\pi\sqrt{1-\left(\frac{\Delta}{\lambda}\right)^2}} \ln\left(\frac{4\left[\left(\frac{\lambda}{\Delta}\right)^2 - 1\right]}{\varepsilon''\left[2\left(\frac{\lambda}{\Delta}\right)^2 - 1\right] + \mu''}\right) \quad (8)$$

The dependence of the cut-off frequency on the thickness of the metamaterial slab was plotted in Fig 3. The cut-off frequency for thinner slabs was increasing sharply. As thickness increased small losses in both ε and μ brought the cut-off frequency down. For thicker slabs the cut-off frequency was approximately equal to k_O so that only very minute improvement in sub wavelength resolution could be achieved. Also, as the thickness of the slab increased, it became more non-transparent for the propagating components which lost more and more energy while propagating through the slab [18].

To design a slab which could produce high resolution, the thickness of the slab should be kept as small as possible. Also, losses in both ε and μ should be kept as low as possible. From Fig 3, we deduced that for $\varepsilon'' = 10^{-3}$ and $\mu'' = 10^{-3}$, the thickness of the slab shouldn't be higher than $d/\lambda = 0.2$. But for $\varepsilon'' = 10^{-1}$ and $\mu'' = 10^{-1}$, the thickness of the slab shouldn't be higher than $d/\lambda = 0.1$ in order to obtain a reasonable cutoff frequency.

3. RESULTS AND DISCUSSION

In this section, through simulation, the possibility of imaging an object that had a dimension equal one over thirty of the wavelength used using a metamaterial slab was studied. The object function at the scattering line was defined. Spatial frequencies were defined for the object function by taking the Fourier transform of it. The total transfer function of the media in which the waves propagated was defined. The Fourier transform of the object function was multiplied by the transfer function of the media and then the inverse Fourier transform was finally calculated. Simulation was done on Matlab™ to examine the success of an actual example of a metamaterial slab in imaging.

3.1 Fourier Transforms and Results Analysis

The object image was in the space domain and the transfer functions were in the frequency domain, so the spatial frequencies of the object image was required to find the effect of propagation in the slab. The Fourier transform was used to relate the space domain and the spatial frequencies domain. The effect of the slab space on the spatial frequencies of the object was obtained by simply multiplying the Fourier

transform of the space domain by the transfer function of the slab. To obtain the image of the object, the inverse Fourier transform of the resulting equation was obtained. Next, we defined two new parameters which were used in evaluating the obtained results in this section.

As shown in Fig 4, the two parameters were the Centre and the FWC (Full Width at Centre). For an image which was obtained for an object, the Centre parameter was defined to be the minimum value of the image curve as shown in Fig. 4. The FWC parameter was the width of the image curve at the value of the Centre parameter. Both parameters were used to evaluate how much an image was identical to the object being imaged.

In this section, we applied Fourier transforms on two cases that were discussed in details in the following subsection. A slab was designed taking into consideration the simulations which were done in section 2. The permeability of the slab which was discussed in this section was equal to one. So, the losses due to variation in permeability were eliminated. The real part of permittivity was equal to negative one so we didn't have to worry about problems from resonances. The only variations assumed were in the imaginary part of the permittivity as well as the thickness of the slab.

3.2 Transfer Functions and Imaging

The ability of a silver superlens to produce images for an object that was much smaller than the wavelength used was investigated. The object of two Aluminum rods each of diameter 1cm was placed at the scattering plane as shown in Fig. 1 (rods not shown). A wave with frequency 3GHz was used. A silver slab was placed in medium2. Silver was an epsilon-negative material with relative permittivity $\varepsilon_r = -1 - 0.01j$. The width of the silver slab was d_2 mm. The object was placed at d_1 mm in front of the surface of the slab. The image was expected to appear at d_3 mm behind the rear surface of the slab.

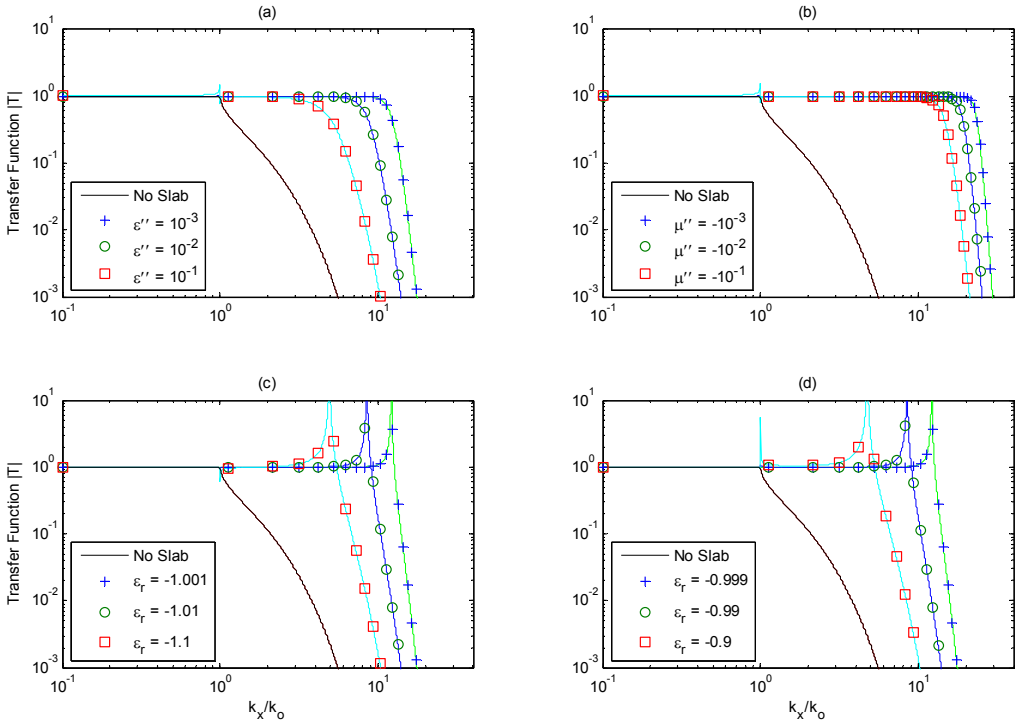

Fig. 2. The plots showed the amplitude of the transfer function when changing the values of the imaginary and real parts of the permittivity and permeability of a metamaterial slab. The amplitude of the transfer function was plotted when the slab was absent for reference

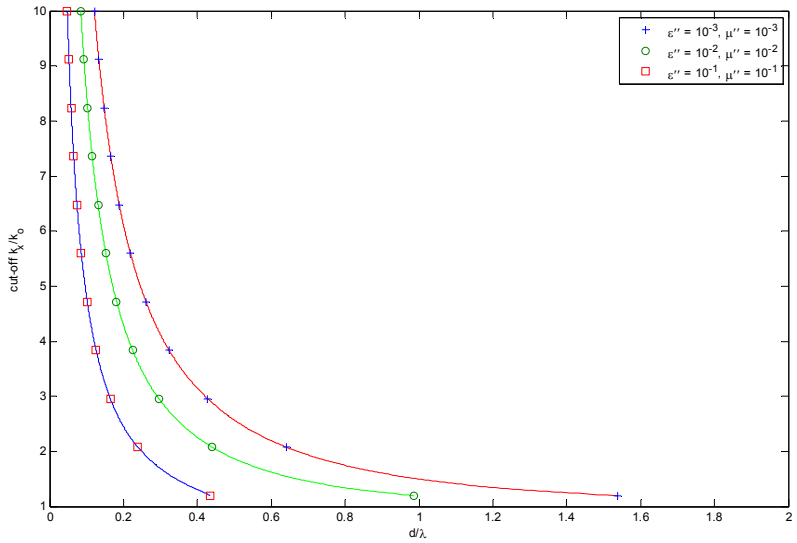

Fig. 3. The plot showed the change in cut-off frequency as the thickness of the slab changed when changing the values of the imaginary parts of the permittivity and permeability of a metamaterial slab

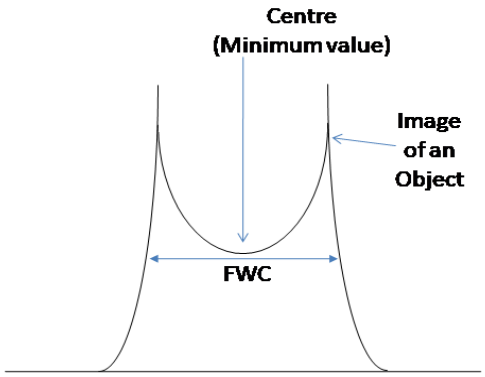

Fig. 4. A sketch of the definition of Centre and FWC which were used to quantify the results in this section

The results were plotted in Fig. 5 and tabulated in Table 1. For the first case, the values $d_2 = 16\text{mm}$ and $d_1 = d_3 = 8\text{mm}$ were used. In Fig. 5a, the amplitude of the transfer function T was plotted in the plot on the right. For $k_x < k_o$, $|T|$ was equal to one which meant that all frequencies which satisfied this range passed through the silver slab without attenuation. For $k_x > k_o$, $|T|$ was almost equal to one up till the cutoff frequency when k_x was almost equal $8k_o$ then $|T|$ attenuated to almost zero. In the plot on the left, the amplitude of the electric field representing the two Aluminum rods were drawn. The object (dotted line) was a two step function of amplitude one and width 1cm. The image (solid line) looked as two parabolic functions joined along the x-axis each with the Centre value equal 0.5999 and the FWC equal to 1.047. The image didn't represent the object being imaged. For the second case, the values $d_2 = 4\text{mm}$ and $d_1 = d_3 = 2\text{mm}$ were used. In Fig. 5b, $|T|$ was equal to one for all frequencies satisfying $k_x < k_o$ in the plot on the right. For $k_x > k_o$, $|T|$ was almost equal to one up till the cutoff frequency when k_x was almost equal $30k_o$ then $|T|$ attenuated to almost zero. In the plot on the left, the object (dotted line) was a two step function of amplitude one and width 1cm. The image (solid line) had the shape of two parabolic functions joined together with the Centre value equal to 0.6000 and the FWC equal to 1.047. The amplitude of the points $x \approx -2$ and $x \approx 2$ increased slightly than those found in Fig. 5a. For the third case, the values $d_2 = 1\text{mm}$ and $d_1 = d_3 = 0.5\text{mm}$ were used. In Fig. 5c, $|T|$ was equal to one for all frequencies satisfying $k_x < k_o$ in the plot on the right. For $k_x > k_o$, $|T|$ was almost equal to one

up till the cutoff frequency when k_x was almost equal $117k_o$ then $|T|$ attenuated to almost zero. In the plot on the left, the image (solid line) had the shape of two step functions representing the object being imaged where each function had the Centre value equal to 0.9606 and the FWC equal to 1.0. The image was a good representative of the object being imaged than those shown in Figs. 5a and 5b. For the fourth case, the values $d_2 = 0.25\text{mm}$ and $d_1 = d_3 = 0.125\text{mm}$ were used. In Fig. 5d, $|T|$ was equal to one for all frequencies satisfying $k_x < k_o$ in the plot on the right. For $k_x > k_o$, $|T|$ was almost equal to one up till the cutoff frequency when k_x was almost equal $931k_o$ then $|T|$ attenuated to almost zero. In the plot on the left, the image (solid line) had the same shape of the object being imaged with the Centre value equal to 1.0 and the FWC equal to 1.0. The image was a perfect representation of the object being imaged. As the thickness of the slab decreased, the range of evanescent frequencies that could be amplified through the slab increased. The evanescent waves captured at the receiver side held detailed information about the object and so the obtained image was more perfect. For good imaging the thickness of the slab should be equal to one tenth the width of the object being imaged or less.

Next the same simulations were repeated as in Fig. 5 while taking the relative permittivity of the slab to be $\varepsilon_r = -1 - 0.4j$. The results were plotted in Fig. 6 and tabulated in Table 2. The first case was shown in Fig. 6a. For $k_x > k_o$, $|T|$ was almost equal to one up till the cutoff frequency when k_x was almost equal $2k_o$ then $|T|$ attenuated to almost zero. In the plot on the left, the image (solid line) looked as two parabolic functions joined along the x-axis each with the Centre value equal 0.5015 and the FWC equal to 1.046. The second case was shown in Fig. 6b. For $k_x > k_o$, $|T|$ was almost equal to one up till the cutoff frequency when k_x was almost equal $8k_o$ then $|T|$ attenuated to almost zero. In the plot on the left, the image (solid line) had two parabolic functions each with the Centre value equal 0.5799 and the FWC equal to 1.046. The amplitude of the points $x \approx -2$ and $x \approx 2$ increased than those seen in Fig. 6a. The third case was shown in Fig. 6c. For $k_x > k_o$, $|T|$ was almost equal to one up till the cutoff frequency when k_x was almost equal $31k_o$ then $|T|$ attenuated to almost zero. In the plot on the left, the image (solid line) had two parabolas each with the Centre value equal 0.5976 and the FWC equal to 1.045. The amplitude of the points $x \approx -2$ and $x \approx 2$ increased than those shown in Fig. 6b. The fourth case was shown in Fig. 6d. For $k_x > k_o$, $|T|$ was almost equal to one up till the cutoff frequency when k_x was almost equal $246k_o$. In the plot on the left, the image (solid line) had the same shape of the object being imaged. The image was a good representation of the object being imaged. Losses had deteriorated the quality of the images being produced using the same thicknesses as those used in Fig. 5.

Table 1. A Table to compare the results which were shown in Fig. 5

Slab Thickness	Centre $\lvert E_x \rvert$	FWC	Cutoff Freq	Image Quality
16 mm	0.5999	1.047	$7.32\,k_o$	Moderate
4 mm	0.6	1.047	$29.08\,k_o$	Moderate
1 mm	0.9606	1	$116.3\,k_o$	Good
0.25 mm	1	1	$930.3\,k_o$	Good

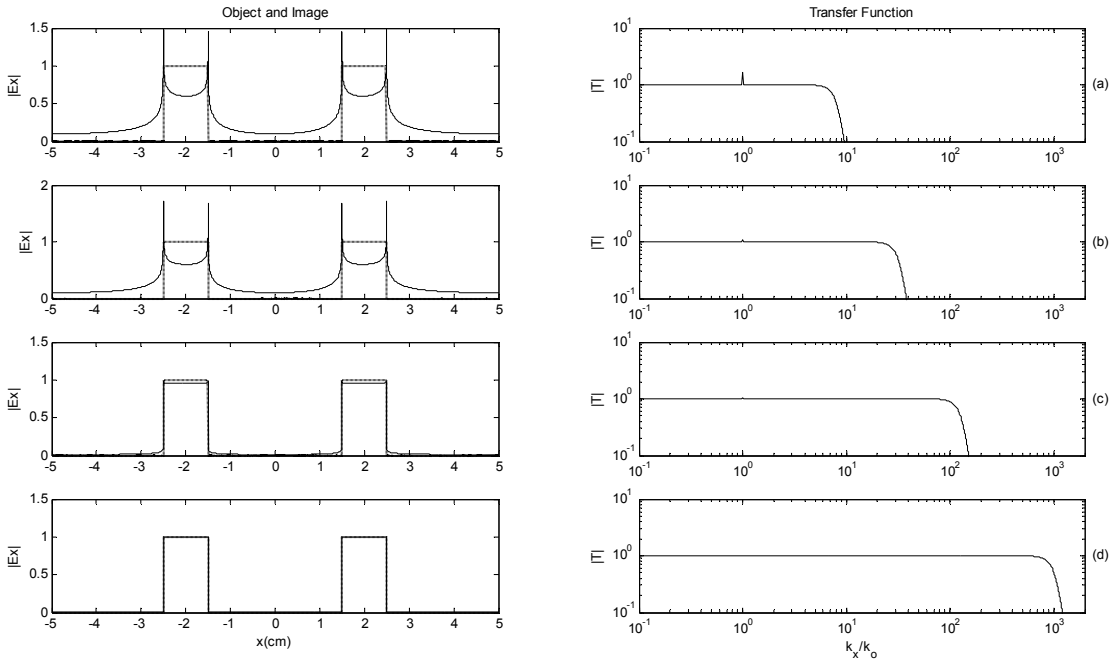

Fig. 5. The plots on the left showed the object electric field (dotted lines) for two Aluminum rods which were placed at the scattering plane as shown in Fig. 1. The solid lines represented the output electric field which was received at the receiver plane as shown in Fig.1. The plots on the right showed the amplitude of the transfer function Eq. 3. The thicknesses of the slab were 16, 4, 1 and 0.25mm in the Figures a-d consecutively. Imaginary part of permittivity was 0.01

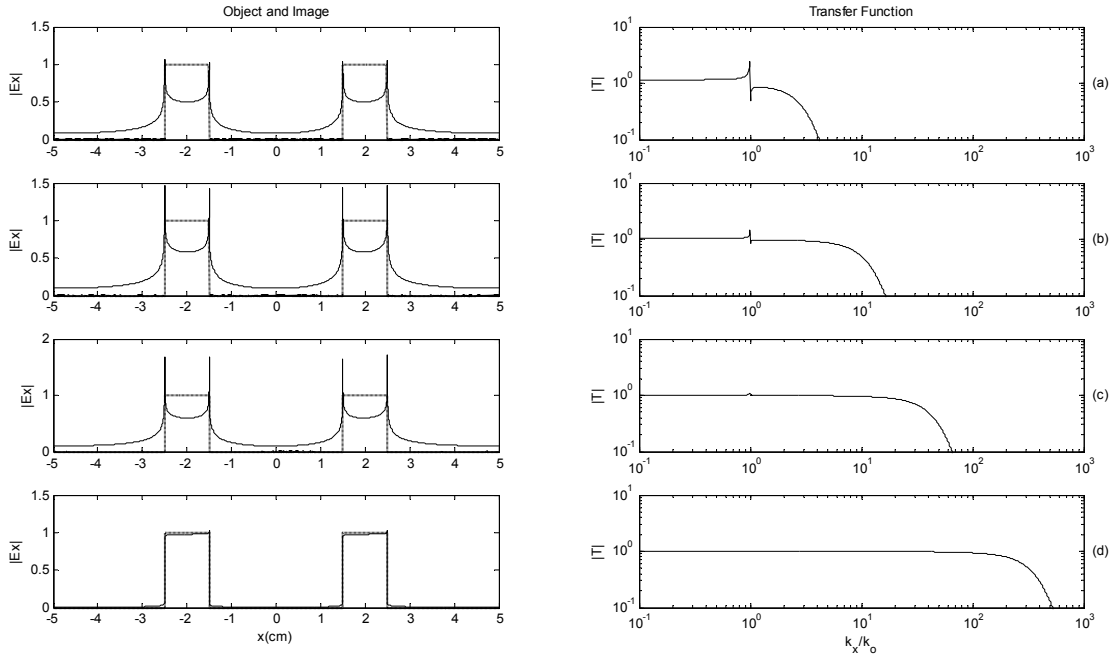

Fig. 6. Same plots as those shown in Fig. 5 but while using an imaginary part of permittivity that was equal to 0.4

Table 2. A Table to compare the results which were shown in Fig. 6

Slab Thickness	Centre $\lvert E_x \rvert$	FWC	Cutoff Freq	Image Quality
16 mm	0.5015	1.046	$1.996\,k_o$	Not good
4 mm	0.5799	1.046	$7.699\,k_o$	Moderate
1 mm	0.5976	1.045	$30.73\,k_o$	Moderate
0.25 mm	0.9748	1	$245.8\,k_o$	Good

4. CONCLUSION

Evanescent waves carried detailed information about the object being imaged but they were fast decaying waves which couldn't be captured at the receiver side. Metamaterial slabs were used to amplify the amplitude of the evanescent waves so that they could be captured using antennas. The variation in the cut-off frequency for a metamaterial slab was examined when changing the real or imaginary parts of the permittivity and permeability of the slab. Increasing the imaginary part of the permittivity reduced the cut-off frequency of the slab. Increasing the imaginary part of the permeability reduced the cut-off frequency as well but with less sensitivity than that for permittivity. When changing the real part of either the permittivity or permeability similar behavior for the cut-off frequency was seen. However; resonance in the amplitude of the transfer function was seen. The cause of these resonances was the excitation of the Surface Plasmon Polaritons (SPP) modes. Next, the relationship between the possible resolution that could be achieved and the thickness of the slab was studied. As the thickness of the slab decreased, the cut-off frequency increased. Also as the thickness of the slab increased, the propagating components of the frequencies lost more energy inside the slab. An investigation had been made to test the possibility of imaging two Aluminum rods by using a silver slab. A slab made out of silver had a permeability value of one and a permittivity value of negative one. All problems discussed in section 2 about the reduction in the cutoff frequency due to losses in permeability or change in the real value of permittivity were eliminated. In the first example, losses in permittivity were low and so a good image representing the object being imaged was retrieved when a slab of thickness 1mm or 0.25mm was used. As the thickness of the slab decreased, the range of evanescent frequencies that could be amplified through the slab increased. The value of the transfer function was almost equal to one for an increasing range of evanescent components as the thickness of the slab decreased. The reason for the amplification was the excitation of Surface Plasmon Polaritons (SPP modes). The scattered waves which were incident on the surface of the slab excited the SPP at the rear side of the slab. These modes gave the effect as if the amplitude was amplified or was increased as waves propagated inside the slab. In the second example losses in permittivity were higher than those used in the first one and so a good image was retrieved when a slab of thickness 0.25mm was used. Losses affected the resolution of the obtained images negatively. We concluded that results showed that for a frequency of 3GHz and an object of diameter 1cm, the slab didn't manage to amplify evanescent waves except in 3 cases. For an imaginary value of permittivity equal 0.01, reasonable resolution was not obtained except when thickness was 1mm or 0.25mm. But for an imaginary value of permittivity equal 0.4, reasonable resolution was not obtained except when thickness was 0.25mm.

ACKNOWLEDGEMENTS

This work was supported by a CONACYT-TWAS Postdoctoral Fellowship (FR number: 3240255079) covered by The National Council on Science and Technology (CONACYT) and The Academy of Sciences for the Developing World (TWAS).

COMPETING INTERESTS

Authors have declared that no competing interests exist.

REFERENCES

1. Harker BJ, Chadwick AD, Harris GL. Ultra-wideband 3-dimensional imaging. Roke Manor Research Limited, UK; 2008. Available:http://www.roke.co.uk/resources/papers/UWB-3D-Imaging.pdf.

2. Kidera S, Sakamoto T, Sato T. Accurate UWB radar three-dimensional imaging algorithm for a complex boundary without range point connections. IEEE Transactions on Geoscience and Remote Sensing. 2010;48(4):1993-2004.
3. Narayanan RM, Xu X, Henning JA. Radar penetration imaging using ultra-wideband (UWB) random noise waveforms. IEE Proceedings - Radar, Sonar and Navigation. 2004;151(3):143.
4. Hassanein, Ahmed MDE. Imaging techniques using ultra wide band waves. Thesis. Oxford University; 2008.
5. Hassanein, Ahmed MDE, Alonso corona chavez improving ultra wide band imaging using a metamaterial slab. International Journal of Computer Applications. 2014; 94(5):38-42.
DOI: 10.5120/16343-5650.
6. Hecht, Eugene. Optics. Fourth edition. reading, MA: Addison-Wesley, 2002. Print.
7. Pendry JB, Anantha Ramakrishna S. Near-field lenses in two dimensions. Journal of Physics: Condensed Matter. 2002;14(36): 8463-479.
8. Aslam Muhammad I, Durdu Oe Gueney. On negative index metamaterial spacers and their unusual optical properties. Progress In Electromagnetics Research B. 2013;47:203-17.
9. Yuan Yu, Bogdan-Ioan Popa, Steven A. Cummer. Zero loss magnetic metamaterials using powered active unit cells. Optics Express. 2009;17(18): 16135.
10. Ramakrishna S. Anantha JB, Pendry D. Schurig D, Smith R, Schultz S. The asymmetric lossy near-perfect lens. Journal of Modern Optics. 2002;49(10): 1747-762.
11. Gallina, Ilaria, Giuseppe Castaldi, Vincenzo Galdi, Andrea Alù, Nader Engheta. general class of metamaterial transformation slabs. Physical Review. B. 2010;81(12):(125124)1-10.
12. Dong, Zheng-Gao, Shuang-Ying Lei, Ming-Xiang Xu, Hui Liu, Tao Li, Fu-Ming Wang, and Shi-Ning Zhu. Negative Index of refraction in metallic metamaterial comprising split-ring resonators. Physical Review E. 2008;77(5):056609(1-4).
13. Roglá LJ, Carbonell J, Ve. Boria. Study of equivalent circuits for open-ring and split-ring resonators in coplanar waveguide technology. IET Microwaves, Antennas & Propagation. 2007;1(1):170.
14. Radkovskaya A, Shamonin M, Stevens CJ, Faulkner G, Edwards DJ, Shamonina E, Solymar L. Resonant frequencies of a combination of split rings: Experimental, analytical and numerical study. Microwave and Optical Technology Letters. 2005;46(5):473-76.
15. Pendry JB, Holden AJ, Stewart WJ, Youngs I. extremely low frequency plasmons in metallic microstructures. Phys. Rev. Lett. 1996;76:4773-776.
16. Lim CS, Hong MH, Chen ZC, Han NR, Luk'Yanchuk B, Chong TC. Hybrid metamaterial design and fabrication for terahertz resonance response enhancement. Optics Express. 2010;18 (12):12421.
17. Schurig D, Pendry JB, Smith DR. Transformation-designed optical elements. Optics Express. 2007;15(22):14772.
18. Solymar L, Shamonina E. Waves in metamaterials. first edition. Oxford: Oxford UP; 2009. Print.

Peer-review history:
The peer review history for this paper can be accessed here:
http://www.sciencedomain.org/review-history.php?iid=969&id=31&aid=8207